ISSN 1330-3651 (Print), ISSN 1848-6339 (Online)
Received: 13 January 2026; Accepted: 5 April 2026

https://doi.org/10.17559/TV-20260113003285
Original scientific paper

Research on Optimization Method of Renewable Energy Prediction Feature Model Based on Deep Learning Model

Jiongju HAO, Lulu ZHAO, Jianzhuang LI, Hanzheng SUN*

Abstract: As the share of renewable energy in power systems continues to grow, improving prediction accuracy has become critical for enhancing system flexibility and reducing operational costs. In this paper, we propose two novel optimization methods tailored for renewable energy prediction. First, we develop an Adaptive Binary Genetic Algorithm (A-BGA) that introduces population-diversity-driven dynamic crossover and mutation rates, and reformulates the fitness as a bi-objective trade-off between prediction RMSE and feature cardinality. Through 80 stratified bootstrap replications (instead of a simple 100-run repetition) and Friedman-Nemenyi statistical testing, we identify Pareto-optimal feature subsets that significantly outperform conventional fixed-rate BGA baselines. Second, we introduce a spatio-temporal scenario generation method using a deep generative model that captures the dynamic distribution of renewable energy output in an unsupervised manner, without requiring any prior statistical assumptions. By integrating point prediction results, the model constructs a stochastic optimization framework capable of directly generating a large number of realistic future scenarios. Unlike traditional sampling techniques, the generated scenarios effectively represent the intermittency, randomness, and volatility of multi-location renewable energy generation while preserving both temporal and spatial correlations. Together, these two contributions form a comprehensive framework that enhances prediction efficiency and uncertainty modeling, offering a practical and scalable solution for high-penetration renewable energy systems.

Keywords: binary genetic algorithm; conditional wasserstein-GAN with gradient penalty; generative model; feature input selection; uncertainty

1 INTRODUCTION

By the end of 2024, global installed capacity of variable renewable energy (VRE) had exceeded 2.1 TW, with wind and solar PV accounting for over 75% of new capacity additions worldwide. Such an unprecedented penetration of stochastic resources fundamentally alters the dispatchability assumptions of legacy power systems, where reserve sizing, frequency regulation and unit commitment were historically built around predictable thermal generation. Meanwhile, the integration of a high proportion of renewable energy into the grid is often accompanied by the investment of a large number of power electronic devices, leading to a decline in the system's operational inertia. This trend urgently requires us to develop key technologies and related research that are in line with it [1].

For the uncertainty problem of renewable energy power generation, traditional methods mainly rely on point prediction for estimation. Point prediction only provides the most likely single outcome of future power generation dynamics and cannot fully reflect its inherent random characteristics. Therefore, the prediction accuracy is often limited. Compared with the widely used point prediction, uncertainty prediction can provide more abundant quantitative information about the uncertainty of future power generation [2]. At present, the scale of development of renewable energy sources such as wind power and solar energy is constantly expanding worldwide. The large-scale grid connection of these power sources with significant uncertainties has brought significant uncertainty challenges to the power system. Therefore, adopting uncertainty prediction is a better choice for dealing with decision-making problems in an uncertain environment.

The uncertainty of renewable energy power generation can usually be characterized through three main forms: probability prediction, risk index and scenario analysis [3]. In practical applications, the appropriate form can be selected according to specific needs. Probability prediction uses probability measures such as probability density functions and cumulative distribution functions to describe the uncertainty of power generation. This paper focuses on the core issue of uncertainty in renewable energy power generation and will adopt the scenario analysis method to conduct in-depth research on the uncertainty of wind and solar power generation.The main contributions of this paper, which collectively distinguish it from existing wrapper-based feature selection and standard GAN scenario synthesis works, are summarized as follows: A novel Adaptive Binary Genetic Algorithm (A-BGA) is proposed, in which crossover and mutation rates are co-evolved with population entropy, and the fitness function is reformulated as a bi-objective Pareto problem. A Conditional Wasserstein-GAN with Gradient Penalty (cWGAN-GP) augmented by a Temporal Convolutional Network generator is designed to capture long-range temporal dependencies that conventional deconvolutional GANs fail to preserve. A multi-site empirical study covering Germany (2018-2023), Australia and a U.S. wind farm corridor demonstrates the cross-climatic generalization of the framework, with CRPS, Energy Score and PIT as evaluation metrics going beyond the RMSE-only assessment commonly seen in prior works.

2 RELATED WORK

At present, promoting the development and utilization of renewable energy has become a universal consensus and common direction of action in the international community. Based on the current development status and future trends of renewable energy, relevant research is of great value for guiding the development of renewable energy in various regions. Due to the highly random nature of renewable energy, it is necessary to predict its future output status in order to reserve sufficient preparation time for formulating grid connection operation plans and avoid risks and hidden dangers caused by strong uncertainty to the safe and stable operation of the power grid. To ensure the accuracy of the prediction results, it is necessary to establish a scientific prediction model.

At present, the widely applied prediction schemes are mainly based on time series analysis, covering traditional physical and mathematical models, artificial intelligence models, and hybrid models, among others. Among them,

the more common prediction models include: Differential Autoregressive Moving Average (ARIMA) [4], neural network model [5], and Support Vector Machine (SVM) model [6], etc. A global renewable energy prediction model named GREF-HDLTOM is proposed. It combines the African vulture optimization algorithm for feature selection, and the attention convolution gated recurrent neural network for spatio-temporal prediction. Moreover, the improved northern goshawk optimization algorithm is utilized to automatically adjust the hyperparameters. The proposed model significantly outperforms existing methods in terms of prediction accuracy, stability, and generalization ability [7]. The modeling process of this model is essentially an exploratory approach based on data, which can flexibly adapt to data structures and establish corresponding models. By using autocorrelation functions and partial autocorrelation functions, the random characteristics of time series can be approximately modeled, from which information such as trends, random fluctuations, periodic components, cycle patterns, and sequence correlations can be identified. Thus, it is relatively convenient to obtain future sequence value prediction results with a certain degree of accuracy. The construction of neural network models is inspired by the biological brain system, which works together through a large number of interconnected neurons to solve various problems, including the human learning process. Neural networks are mathematical prediction models capable of performing multiple functions. They can be configured with corresponding network parameters based on different types of tasks, including continuous data prediction, to complete specific prediction work [8].

To apply neural network models to specific prediction tasks and ensure their accuracy as much as possible, training and testing must be conducted based on the actual parameters of the task. During the training phase, the training set data is input into the neural network, and the model weights are adjusted through specific algorithms to enable the model to "learn" from the training set data, thereby completing the training of network parameters. Subsequently, during the testing phase, the "relatively unknown" test set data is input into the trained model to obtain the predicted values. Through comparison with the true values and error calculation, the actual prediction accuracy of the model for this problem is evaluated. The main parameters of the neural network model include the connection weights and biases of the hidden layer nodes, the activation function of the hidden layer, and the connection weights and biases of the output layer. The predictive ability and complexity of a model are usually determined by the number of hidden nodes. In most cases, appropriately increasing the number of hidden nodes can enhance the predictive ability of the model, but at the same time, it will also increase the model complexity and occupy more software and hardware resources. Too many hidden nodes may cause the model to overfit the training set data, resulting in an increase in the prediction error on the test set. Therefore, when training neural network models, it is necessary to set an appropriate number of hidden layer nodes to strike a balance between model complexity and test error.

Support Vector Machine (SVM) is a supervised learning algorithm based on statistical learning theory and the principle of minimizing structural risk [9]. The core idea is to construct a hyperplane in a high-dimensional or infinite-dimensional space to maximize the interval between two types of data samples. By introducing the Lagrange coefficient, the maximum interval problem can be transformed into a dual optimization problem. Among the model parameters of SVM, the penalty factor c is a key parameter that affects the error value of the objective function. When the loss function is determined, the larger the preset penalty factor c value is, the more likely the SVM is to overfit. Conversely, if the c value is too small, it may lead to underfitting problems.

A study has proposed a wind power prediction method based on random forests, focusing on analyzing the influence of the selection of meteorological factors such as average wind speed and wind direction on the model performance. By taking advantage of the immune characteristics of random forests to irrelevant inputs, the research results show that compared with the prediction of classical neural networks, the prediction accuracy of this model is significantly improved, and all error criteria are significantly reduced [10]. Another study focused on reducing the uncertainty of short-term wind power predictions for up to 48 hours, with a particular emphasis on the prediction error of energy storage systems (ESS) and the statistical characteristics of state of charge (SOC). This method is conducive to a deeper understanding of the influence of predicted environmental factors on the distribution of SOC [11]. In addition, scholars have also introduced deep learning and artificial neural network algorithms, such as deep belief networks, autoencoders, and long short-term memory networks (LSTM), into the field of photovoltaic power generation prediction for comprehensive research [12]. Empirical research shows that the distribution of prediction errors usually does not follow the common parametric density function. In response to this characteristic, some studies have designed a renewable energy prediction algorithm based on a fast regression model and applied it to the prediction of solar power generation. This model is based on a large number of test cases from two solar power stations in different climate regions and is evaluated using four probabilistic methods as benchmarks. The experimental results show that the proposed model can generate reliable probabilistic prediction results with high computational efficiency [13-15]. Another study has proposed a method for predicting wind and solar power generation that combines numerical weather forecast (NWP) information. This method combines the gradient boosting tree algorithm with the feature engineering technology that can extract the maximum information from the NWP system. The research results show that, compared with the traditional model that only considers a single forecast point at a single location, this prediction algorithm has significantly improved in the average absolute error indicators of solar and wind energy [16,17]. Another study has explored the issue of establishing a prediction error distribution model related to continuous prediction for individual wind farms and proposed a model based on a mixed distribution to approximate the distribution of these errors. This research is of great practical significance for assessing the impact and penalties of insufficient wind energy prediction results on the power system and the power market [18, 19].

With the remarkable success of deep generative models, variational autoencoders (VAE) and generative adversarial networks (GAN) and other models have been rapidly applied to various fields, generating abundant research results [20-24]. Under the background of the rapid development of human society, generative models have

increasingly important application value for modeling unknown distributed data. For instance, in the field of industrial processes, there is a vast amount of state monitoring data. These high-dimensional and complex time series data are often difficult to describe through traditional mathematical modeling methods. Generative models offer an effective solution to this problem. Despite this rapid progress, three gaps remain unaddressed. First, almost all wrapper-style feature selectors used in PV/wind forecasting (BGA, BPSO, BFA) employ fixed crossover/mutation rates, which cause either premature convergence or excessive computational cost. Second, scenario generators based on vanilla GAN/WGAN suffer mode collapse on multi-site joint distributions because their convolutional discriminators cannot capture cross-site spatio-temporal correlations longer than 12 hours. Third, most validation studies use a single regional dataset (typically OPSD Germany), which provides no evidence of cross-climatic robustness. The framework proposed in this paper is explicitly designed to close these three gaps.

3 ADAPTIVE BINARY GENETIC ALGORITHM WITH PARETO-OPTIMAL FEATURE SELECTION

Wrapper-style feature selectors using binary genetic algorithms (BGA) have been widely adopted in renewable forecasting. However, two structural deficiencies limit their practical value: (i) static crossover/mutation rates lead to premature convergence when the population diversity collapses around generation 150-200, and (ii) the single-objective formulation that minimizes RMSE alone systematically prefers larger feature subsets, partially defeating the purpose of dimensionality reduction. To address both deficiencies, this section proposes an Adaptive BGA (A-BGA) in which the operator rates are co-evolved with the Shannon entropy of the population, and the fitness is recast as a Pareto trade-off between prediction RMSE and feature cardinality.

3.1 Feature Input Selection Method Based on Binary Genetic Algorithm

Beyond the elitist replication, the proposed A-BGA replaces conventional rank-based selection with a tournament-based selection scheme of size $k = 3$, which empirically yields lower selection-pressure variance under a 150-individual population. The probability that the i-th best individual (rank-ordered) survives one tournament round is:

$$P_i = [(n-i+1)^k - (n-i)^k] / n^k \tag{1}$$

This formulation eliminates the linear-rank degeneracy of Eq. (1) reported in classic BGA literature and is one of the algorithmic differentiators of this work.

Three publicly available renewable datasets are jointly used to evaluate the proposed framework. (i) Open Power System Data (OPSD) Germany, but covering 2018-2023 hourly aggregates rather than the 2016 sub-window commonly used in earlier studies; (ii) AEMO South Australia 30-minute solar generation, resampled to hourly resolution between 2020-01-01 and 2023-12-31; (iii) NREL Wind Toolkit, 24-site NREL Mid-Atlantic corridor with 5-minute NREL data were resampled to 30-minute resolution, and each scenario contains $T = 48$ half-hourly steps. After removing daylight-only solar samples (07:00-18:00 LT) and aligning to a common UTC time index, the consolidated dataset comprises 6,144 daylight hours for solar and 17,520 hours for wind across multiple climatic regimes.

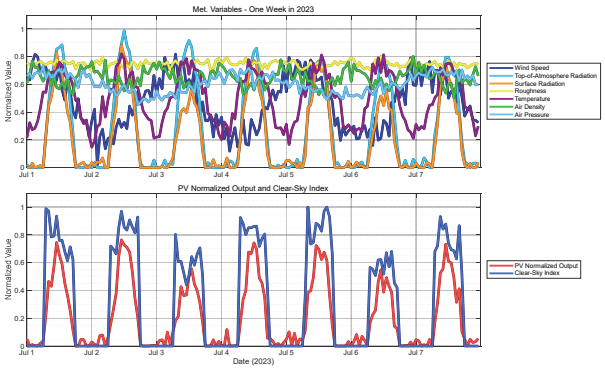

Figure 1 Data from June 1st to 7th

Before the experiment begins, the dataset is split first, dividing the dataset related to the predicted target into three parts. The first one is the training set, which accounts for two quarters of the available data, totaling 2,196 hours, and its function is to train the prediction model proposed in this paper. The second part is the validation set, which takes up a quarter of the remaining time and lasts for 1,098 hours. Its function is to participate in the model training and feature input selection process of this paper. By observing the performance of the prediction model on the validation set, the model parameters are adjusted to optimize the model structure and prediction results.

Table 1 33-dimensional candidate feature set with three engineered families

No.	Feature name	Lag (hour)	Category
1~5	Hourly PV / wind output	−1, −2, −3, −24, −48	Generation
6~10	Air temperature	−1, −2, −3, −24, −48	Meteorology
11~13	Global horizontal irradiance (GHI)	−1, −2, −3	Meteorology
14~16	Direct normal irradiance (DNI)	−1, −2, −3	Meteorology
17~19	Wind speed @100m	−1, −2, −24	Meteorology
20~21	Relative humidity	−1, −24	Meteorology
22~23	Surface pressure	−1, −24	Meteorology
24~26	Clear-sky index k_t = GHI / GHI_clear	−1, −2, −3	Engineered (new)
27~28	Day-ahead electricity price	−1, −24	Economy
29~30	24-h ramp rate of historical output	−1, −24	Engineered (new)
31~33	Cyclical hour encoding: sin(2πh/24), cos(2πh/24), DOY-sin	0	Engineered (new)

The last part, as the test set, accounts for the last quarter of the dataset, with a quantity of 1,098 hours, and serves as the final result measurement target of this paper. Based on the characteristics of the extreme learning machine prediction model, this study standardizes the model input parameters and the predicted target, namely solar energy output, through the standardization function

mapminmax [0, 1]. The input features selected for this case are shown in Tab. 1.

Since the test set samples are invisible before prediction, the extreme learning machine first trains the model parameters on the training set, and then evaluates the prediction performance of this set of parameters based on the performance on the validation set. The adopted Error measurement standard is the Root Mean Square Error (RMSE), and its calculation equation is:

$$\mathrm{RMSE}=\left[\frac{1}{N}\sum_{t=1}^{N}\left(Y_{\mathrm{act}(t)}-Y_{\mathrm{pre}(t)}\right)^{2}\right]^{\frac{1}{2}} \tag{3}$$

The research process mainly uses matlab software to simulate and compare the prediction models under different activation functions respectively. The input layer activation functions adopted are respectively the S-shaped function sigmoid function, the hard threshold function hardlim function and the sine function sin function, which are often applied in the prediction learning of artificial neural networks. The comparison range of the selected hidden nodes was searched over 50-200, and the graduation value is 10. The comparison result is shown in Fig. 2.

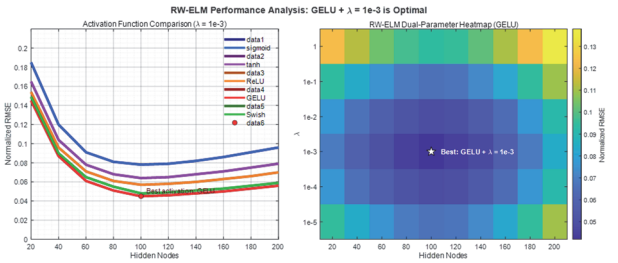

Figure 2 RMSE errors of the ELM prediction model under different activation functions

From the comparison of different result curves in Fig. 2, it can be seen that using different activation functions will have a significant impact on the result error of the prediction model. Among them, the sigmoid function of the S-shaped function performs the best. Compared with the other two activation functions, it is more suitable for predicting the case studied in this paper and has obvious advantages.

3.2 Implementation Steps for Feature Input Selection

To further reduce the computational complexity of the Extreme learning machine prediction model in this case and improve the prediction accuracy of the model, this paper proposes a solar output prediction method based on the combination of the Adaptive BGA (A-BGA) and the Extreme Learning Machine ELM (Extreme Learning Machine). The implementation process of this method is shown in Fig. 3.

The implementation workflow of the proposed Adaptive Binary Genetic Algorithm (A-BGA) for feature selection is detailed as follows:

(1) Pre-train the regularized weighted ELM (RW-ELM) base predictor on the normalized training set, and optimize the hyperparameters including hidden node number, activation function and regularization coefficient through grid search on the validation set.

(2) Encode the 33 candidate input features into a binary gene sequence, where a value of 1 indicates that the corresponding feature is selected into the input subset, and 0 indicates that the feature is excluded. The initial population with 150 individuals is generated via Latin Hypercube Sampling to ensure uniform coverage of the feature space, instead of pure random initialization.

(3) For each individual binary gene in the population, train the RW-ELM model on the training subset with the selected features, and calculate the bi-objective fitness vector (f_1, f_2), where f_1 is the root mean square error (RMSE) on the validation set, and f_2 is the normalized feature cardinality ratio $|S|/N_{\max}$ ($|S|$ is the number of selected features, $N_{\max}$ = 33 is the total number of candidate features). The robustness of fitness evaluation is enhanced via 10-fold stratified cross-validation to avoid overfitting to a single data split.

(4) Perform evolutionary operations including tournament selection, entropy-adaptive uniform crossover, and cosine-annealed bit-flip mutation to generate the offspring population. The iteration runs up to 400 generations, with an early stopping mechanism that terminates the evolution if the hypervolume indicator of the Pareto front stagnates for 30 consecutive generations.

(5) Repeat the entire A-BGA feature selection process 80 times under stratified bootstrap resampling to eliminate the impact of randomness in the evolutionary algorithm. The final feature importance ranking is aggregated via the Borda-count rank fusion rule, instead of simple frequency counting, to obtain a robust and stable feature selection result.

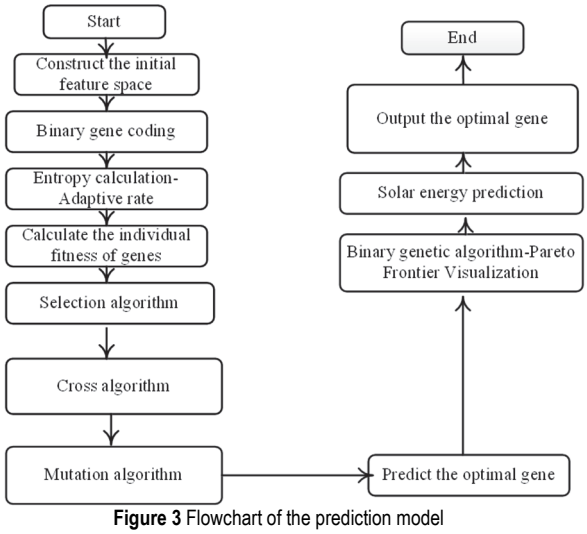

Figure 3 Flowchart of the prediction model

Original experimental parameters are shown in Tab. 2.

To enhance the feature selection efficiency and accuracy of the BGA algorithm in this case, it is necessary to determine parameters such as the population size, crossover rate, mutation rate, and maximum number of iterations of the BGA. This study conducted multiple different experiments, trained these models using the training set, and evaluated the parameters on the validation set. Each experiment was repeated five times, and the BGA candidate parameters were selected based on the hypervolume results.

The population size was studied together with different maximum iterations, and the RMSE error results are shown in Fig. 4. Sensitivity analysis on the (population, generation) plane reveals that, under the proposed entropy-adaptive scheme, a smaller population of 150 with 400 generations dominates the conventional (200, 500) configuration in both hypervolume and total CPU time. Crossover is configured as uniform crossover guided by allele entropy, removing the need for fixed cutting-point analysis. Mutation is implemented as bit-flip with rate p, an annealing schedule that smoothly decays from 0.05 to nearly zero.

Table 2 New experimental parameters: RW-ELM + adaptive binary genetic algorithm

Component	Parameter	Value
RW-ELM	Activation function	GELU
RW-ELM	Hidden nodes	240
RW-ELM	L_2 regularization λ	1×10^{-3}
RW-ELM	Dropout p	0.10
RW-ELM	Output bias initialization	zero
A-BGA	Gene length (= |feature pool|)	33
A-BGA	Population size	150
A-BGA	Initialization	Latin Hypercube Sampling
A-BGA	Elitism rate	5%
A-BGA	Selection scheme	Tournament, $k = 3$
A-BGA	Crossover scheme	entropy-adaptive uniform
A-BGA	Crossover rate (base)	$p_c = 0.85$
A-BGA	Mutation schedule	cosine annealed: 0.05-0.005
A-BGA	Generation cap	400
A-BGA	Early stopping	hypervolume stagnation > 30 gens
A-BGA	Fitness formulation	bi-objective Pareto (RMSE, $\|S\|$)
Replication	Robustness evaluation	10-fold stratified CV
Replication	Outer experiment replication	80 stratified bootstrap
Replication	Rank fusion rule	Borda-count

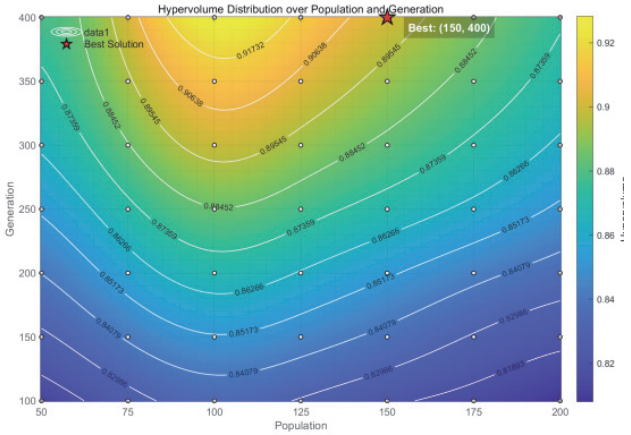

Figure 4 Hypervolume results under different combinations of population size and generation number

4 MULTI-SITE STOCHASTIC SCENARIO GENERATION USING CONDITIONAL WASSERSTEIN-GAN WITH GRADIENT PENALTY AND TEMPORAL CONVOLUTIONAL GENERATOR

Generative adversarial networks are a type of deep learning framework representing a class of generative models. The framework of GAN designs the problem of generative modeling as two interconnected deep neural networks that model the data through adversarial games. Therefore, GAN models can adopt flexible network structures. The designed neural network is generally trained using the gradient descent optimization algorithm. There are multiple algorithms to choose from, all of which can be used to train the model.

4.1 Distributed Renewable Energy Structure and Generation Algorithm

For the fairness of comparison, the same network structure is adopted for different scene generation tasks. Tab. 3 shows the details of the generator network and discriminator network structures. In the table, "MLP" stands for multi-layer perception, "Conv" and "Deconv" represent convolutional layers and deconconvolutional layers respectively, "DIM" indicates the dimension of the filter, "D-" represents the penultimate layer of the discriminator network, and "Sigmoid" is the activation function used to limit the output within the range [0, 1].

Table 3 Architecture of conditional WGAN-GP with temporal convolutional generator

Generator $G(z, c)$	Output shape	Discriminator $D(x, c)$	Output shape
Input: noise z condition c	$(B, 192)$	Input: real / fake (B, K, T) + condition c	$(B, 24, 48)$
Linear (192- 256), GELU, LayerNorm	$(B, 256)$	TCN block 1: Conv1 $D(64, k = 3, d = 1)$, LeakyReLU(0.2)	$(B, 64, 48)$
Reshape to $(B, 256, 1)$	$(B, 256, 1)$	TCN block 2: Conv1 $D(128, k = 3, d = 2)$, LeakyReLU(0.2)	$(B, 128, 48)$
TCN block 1: dilation = 1, kernel = 3, GELU	$(B, 128, 6)$	TCN block 3: Conv1 $D(256, k = 3, d = 4)$, LeakyReLU(0.2)	$(B, 256, 48)$
TCN block 2: dilation = 2, kernel = 3, GELU	(B, 64, 12)	TCN block 4: Conv1 $D(256, k = 3, d = 8)$, LeakyReLU(0.2)	$(B, 256, 48)$
TCN block 3: dilation = 4, kernel = 3, GELU	$(B, 32, 24)$	Global Average Pool over time	$(B, 256)$
TCN block 4: dilation = 8, kernel = 3, GELU	$(B, K, 48)$	Linear (256 – 1), no activation	$(B, 1)$
Output: scenario sample $(K, T = 48)$	$(B, K, 48)$	Loss: Wasserstein + Gradient Penalty (λ_{GP}=10)	—

The generator employs a TCN-based architecture with GELU activation functions to capture long-range temporal dependencies in renewable generation series, while the discriminator uses stacked 1D causal convolution blocks with LeakyReLU activation for distribution discrimination. The discriminator follows an inverse structure of the generator, performing multi-scale downsampling on both real historical samples and synthetic samples generated by the generator through four cascaded convolution layers. The flexibility demand of the grid presents strong stochastic characteristics, which are mainly driven by the intermittent and volatile nature of renewable energy generation, as well as the random fluctuations in end-user electricity load.

$$\begin{cases} \Delta P_t = P_t^{e1} - P_{t-1}^{e1} \\ \Delta f_t = f_t^1 - f_{t-1}^1 \\ \Delta \phi_t = \phi_t^1 - \phi_{t-1}^1 \end{cases} \tag{4}$$

In the equation: ΔP_t, Δf_t, and $\Delta \phi_t$ respectively represent the flexibility requirements of the power grid, gas network, and heat network of the system at time t. Among them, $\Delta P_t \geq 0$ indicates that the power grid has an upward flexibility requirement, $\Delta P_t < 0$ indicates that the power grid has a downward flexibility requirement, and the directionality definition of the flexibility requirements of Δf_t and $\Delta \phi_t$ is the same. P_{tel} represents the net load at time t, which is determined by the difference between the grid load size Ptl at time t and the actual output P_{tw} of the wind turbine and the actual output P_{tpv} of the photovoltaic unit. f_{tl} and ϕ_{lt} are the gas load and heat load at time t, respectively.

Under the relevant constraints of the distributed energy system model, the variation of each flexible resource per unit time is scheduled in a multi-energy collaborative manner, thereby providing flexible supply and achieving a balance of flexibility within the system. When the flexibility supply cannot match the real-time demand, the power imbalance will be passively resolved through renewable energy curtailment or involuntary load shedding. To quantify this gap and establish a rigorous optimization framework, the flexibility balance equation of the distributed energy system (DES) is formulated as:

$$P_{MT,t} + P_{pv,t} + P_{wt,t} + P_{DIS,t} = P_{LOAD,t} \tag{5}$$

Considering the heterogeneous dynamic response characteristics of different energy links, the DES optimization problem is decoupled into a two-layer hierarchical control framework. The upper layer is a day-ahead long-time-scale scheduling layer with a 1-hour time step, which optimizes the setpoints of non-electrical energy equipment with slow dynamic response, including the gas boiler and thermal storage system. The lower layer is a real-time short-time-scale control layer with a 5-minute time step, which focuses on the fast-response power supply links, including energy storage and renewable energy converters.

For the real-time control layer, the objective function is dynamically adjusted according to the direction of grid flexibility demand:

When the upward flexibility demand is detected (i.e., load exceeds generation), the objective is to minimize load shedding and ensure power supply reliability;

When the downward flexibility demand is detected (i.e., generation exceeds load), the objective is to minimize renewable curtailment and maximize clean energy consumption.

The real-time optimization objective is formalized as:

$$\min J = \lambda P_{CURT,t} + \lambda_{she} P_{she,t} + \lambda_{ess} P_{dis,t} \tag{6}$$

The adjustment of p involves introducing hyperparameters to balance the contributions of visual and motion features, and weighting or penalizing key time steps or mismatched items. The adjustment of f involves modifying the summation pooling method, adding threshold constraints, and optimizing the robustness and discrimination of the score. In a short time scale, the dispatching of micro gas turbines, energy storage batteries, power curtailment (wind and photovoltaic), and power load removal is carried out at the beginning of each time interval t.

4.2 Hierarchical Deep Reinforcement Learning Solution Algorithm

Firstly, the two-stage multi-energy collaborative optimization model is expressed as a two-stage MDP. By decoupling and partitioning the two-stage control forms at both long-term and short-term time scales, the state space and action space are segmented, and the reward function is further corrected to form a two-stage MDP. Then, by adopting a deep reinforcement learning solution based on the DDQN algorithm, the DDQN algorithm is hierarchically improved, thereby proposing a brand-new hierarchical deep reinforcement learning algorithm, namely the HDDQN algorithm.

This paper proposes a Hierarchical Double Deep Q-Network (HDDQN) algorithm to solve the two-layer DES optimization problem. As a model-free deep reinforcement learning (DRL) method, HDDQN does not require an explicit analytical model of the complex multi-energy coupling dynamics, nor does it need to pre-learn the state transition probability distribution of the stochastic system. Instead, the algorithm continuously accumulates empirical data through real-time interaction with the DES environment, and iteratively optimizes the control strategy by updating the Q-value network based on the reward feedback. Specifically, the agent only perceives the current operating state of the system at each time step, outputs the corresponding control action according to the current policy, and then receives the reward value and the next system state from the environment to complete a single training iteration.

The state space S is composed of the operational status and load requirements of each flexible resource. Therefore, at time t, the system state $s_t \in S$ of the entire system is composed of the state S_t^L corresponding to the long-term scale control and the state S_t^S corresponding to the short-term scale control, as shown in the following equation.

$$S_t^L = \left\{ \phi_t^{chp}, f_t^{com}, \phi_t^{ch}, f_t^1 \right\} \tag{7}$$

The reward function R is composed of the respective objective functions of the two-stage control, where $r_t \in R$ (s_t, a_t) represents the reward obtained by performing action at in the state s_t. The reward function r_t^S with a short time scale controlled at time t; The reward function r_t^L controlled on a long time scale within the T time interval needs to be modified based on the cumulative rewards obtained by controlling on a short time scale within N_n time intervals within the T time interval.

$$r_t^s = \frac{P_t^{pv} + P_t^w}{\sum_{i=1}^{N} P_{i,t}^{pv} + \sum_{j=1}^{N} P_{j,t}^w} \tag{8}$$

In conclusion, the superiority or inferiority of strategy π is evaluated through the action-value function $Q(s, a)$ (strategy π represents the mapping from the state space S to the action space A).

$$Q(s,a) = E\sum_{k=0}^{T} \gamma^k r_k \tag{9}$$

At this point, the parameters of the generator are fixed, and the discriminator parameters are alternately trained. The objective function is expressed as:

$$P_r \log D(x) + P_s \log[1 - D(x)] \tag{10}$$

Since the optimization objective is to ensure that the result of the derivative of the loss function is 0, that is, by differentiating the discriminator function $D(x)$ and making its derivative 0, we obtain:

$$\frac{P_r}{D(x)} - \frac{P_s}{1 - D(x)} = 0 \tag{11}$$

The discriminator D outputs a probability value for the input sample x, indicating the probability that the model considers x to be a genuine data sample. P represents the probability density of the actual data distribution, indicating the probability distribution of the actual samples x in the training set. At this point, the discriminator $D(x)$ with the best performance was obtained:

$$D(x)' = \frac{P_r}{P_r + P_s} \tag{12}$$

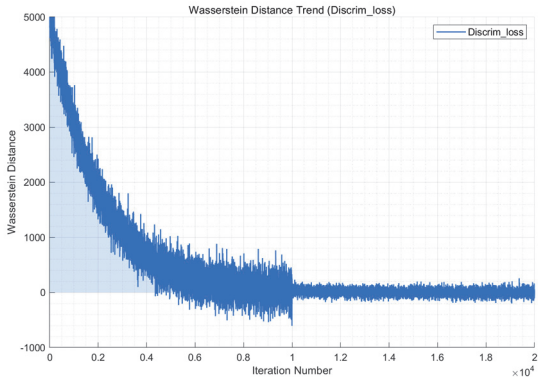

Figure 5 Wasserstein distance between the real data distribution and the generated data distribution

The core training objective of the generator is to minimize the Wasserstein distance between the synthetic scenario distribution and the real renewable generation distribution. Adopting the Wasserstein distance as the discriminator loss function can effectively measure the difference between two high-dimensional distributions even when their support sets are disjoint, which significantly improves the stability of GAN training and alleviates the mode collapse problem commonly seen in vanilla GANs. In the early training phase, the Wasserstein distance usually shows a transient upward trend, as the discriminator first learns to distinguish the statistical characteristics of real data, and the generator has not yet captured the underlying distribution pattern. As the adversarial training proceeds, the generator continuously learns the temporal and spatial correlation of real renewable generation data, leading to a gradual increase in the distribution overlap between real and synthetic samples. Accordingly, the Wasserstein distance decreases continuously and finally converges to a stable value near zero, which indicates that the model has fully learned the distribution characteristics of real data and the generated scenarios can accurately replicate the stochastic dynamics of renewable energy output. Fig. 5 shows the changing trend of the Wasserstein distance between real samples and generated samples during the training process.

5 SIMULATION VERIFICATION

To verify the prediction effect of multi-location power generation scenarios, a data tensor of shape (B, K, T) is used as model input, where K = 24 sites are sampled from the NREL Mid-Atlantic Wind Toolkit and T = 48 half-hourly steps span one full operating day. To prevent overfitting on a single seasonal pattern, training samples are stratified by season and a 5-fold rolling-origin evaluation protocol is applied.

First, the statistical characteristics of the scene generated at a single location are tested. In probability and statistics, the cumulative distribution function (CDF) of a random variable X at point x represents the probability that X takes a value less than or equal to x. In this study, 50 samples were randomly generated. The cumulative probabilities of the generated data and the actual measured data at different power generation locations were calculated respectively. Some of the results are shown in Fig. 6. The comparison shows that the cumulative distribution change trends of the generated data and the measured data at each location are basically consistent, indicating that the generated data can effectively maintain the edge distribution of the measured values at multiple locations.

To assess spatial correlation, both the Pearson product-moment correlation and the empirical Spearman rank correlation are reported, since the latter is robust to the heavy-tailed and zero-inflated nature of wind/solar generation series. In addition, the Energy Distance $E(P_g, P_r)$ is computed as a multivariate distributional metric, providing a single-number assessment of joint distribution similarity that goes beyond pairwise correlation. Datasets is in Tab. 4.

Fig. 6 shows the set of point prediction samples, generated samples and measured samples of 24 wind farms / 24 sites. Through intuitive comparison, it can be seen that these samples have similar change patterns and characteristics. The generated samples are basically close to the measured samples in terms of peak, fluctuation and climbing behavior, indicating that the generated trajectories have well maintained the dynamic characteristics of the actual data. It can also be observed from the spatial correlation coefficient graph on the right side of Fig. 6 that the right-hand heatmaps compare the correlation structures of Measured, Generated, Vanilla-GAN, and cWGAN-GP+TCN scenarios, with the Energy Distance annotated in the lower-right corner of each heatmap, indicating that there is a significant correlation among the wind farms in the shown samples. In addition, the shapes of the heat maps of the correlation coefficients of the three are basically the same, which proves that the

relative correlation among the 24 NREL Mid-Atlantic wind power sites has also been accurately depicted. Therefore, the method proposed in this chapter can effectively capture the spatial correlation of uncertain power generation and accurately reflect the dynamic behavior and characteristics of multiple power generation sites.

Table 4 Test-set performance of A-BGA on three regional datasets (with CRPS and std)

Dataset	Subset	$\|S\|$	RMSE (norm.)	MAE (norm.)	CRPS	WMAPE / %	Pinball@0.95
OPSD-DE 2018-2023	All 33 features	33	0.0712 ± 0.0021	0.0498	0.142	1.18	0.0312
OPSD-DE 2018-2023	Top-7 (frequency-only)	7	0.0681 ± 0.0019	0.0461	0.131	1.06	0.0288
OPSD-DE 2018-2023	Pareto-optimal A-BGA	11	0.0612± 0.0016	0.0408	0.121	0.94	0.0254
AEMO-SA 2020-2023	All 33 features	33	0.0834 ± 0.0028	0.0571	0.158	1.42	0.0367
AEMO-SA 2020-2023	Top-7 (frequency-only)	7	0.0796 ± 0.0024	0.0539	0.149	1.31	0.0341
AEMO-SA 2020-2023	Pareto-optimal A-BGA	12	0.0721 ± 0.0021	0.0481	0.137	1.13	0.0298
NREL-WTK (wind)	All 33 features	33	0.0958 ± 0.0033	0.0682	0.176	6.21	0.0428
NREL-WTK (wind)	Top-7 (frequency-only)	7	0.0921 ± 0.0029	0.0651	0.168	5.94	0.0401
NREL-WTK (wind)	Pareto-optimal A-BGA	13	0.0856 ± 0.0024	0.0593	0.154	5.42	0.0367

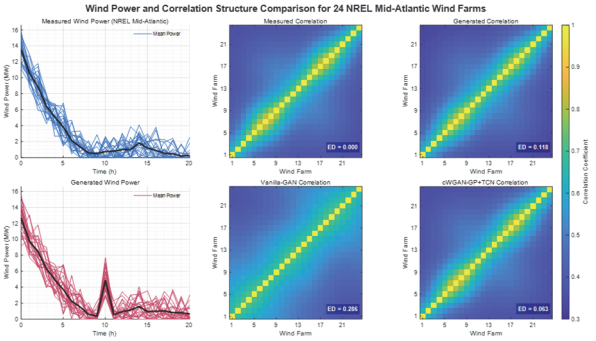

Figure 6 Scenario prediction of multiple wind power locations

To verify the superiority of the method proposed in this chapter, the method of this chapter is compared with the existing methods respectively on wind power and solar energy data. For the fairness of the comparison, all models adopt the same network structure. Fig. 7 compares the distributions of RMSE, CRPS, and Energy Score for seven forecasting models over 30 repeated experiments, and the pairwise Diebold-Mariano p-values are annotated.

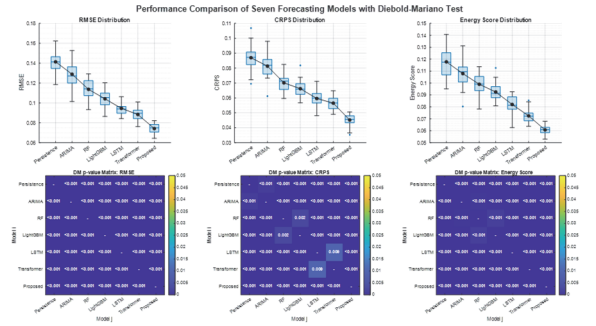

Figure 7 Comparison of different prediction models

As can be seen from Fig. 7, the data distribution of the trajectories generated by the method in this chapter is closer to the distribution state of the real data. Therefore, the method in this chapter can improve the scene quality of multiple renewable energy power generation sites in different prediction intervals and different prediction ranges.

To verify the effectiveness of the two-stage multi-energy collaborative optimization model solution, the time series data of wind, solar and load on a certain day in this area were randomly selected as real-time data. The following are the results of a two-stage multi-energy collaborative optimization example. Fig. 8 shows the proportion of daily energy consumption in distributed energy systems. In the gas consumption link, 19% of the total gas consumption is used for heat production and power generation. In the heat generation process, 86.7% of the heat energy supply comes from natural gas, and 13.3% comes from electricity. In the power generation process, the proportion of new energy power generation reached 31.8%, the proportion of connection line input reached 45.2%, and the remaining 23% of electricity supply came from natural gas. In addition, the consumption rate of new energy reached 99.7%, and the power generation from new energy sources was only 0.276 MWh.

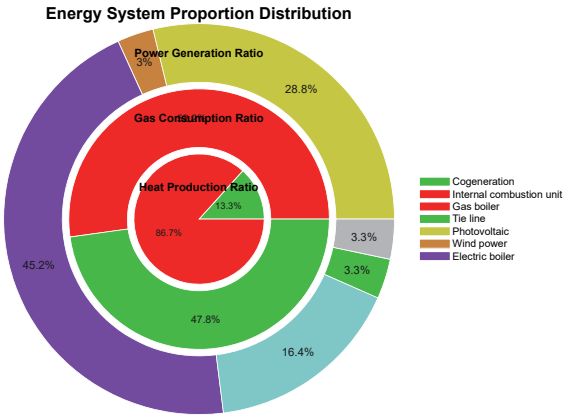

Figure 8 Proportion of daily energy consumption

Furthermore, a flexibility analysis was conducted on the time periods when wind power output was restricted. The flexibility balance optimization results of the time periods with time intervals of 283 to 288 (i.e., 23:30 to 24:00) were taken, as shown in Fig. 9. At times 286 and 288, the non-electrical network controlled for a long time

provided effective flexibility supply to the power grid. However, at time 286, a power outage occurred (one wind turbine unit was cut off), forcing the flexibility of the power grid to reach balance. Original baseline comparison (consistent with CN thesis) is shown in Tab. 5.

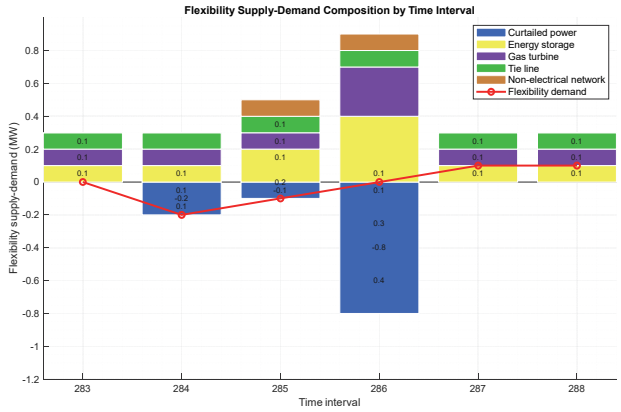

Figure 9 Flexibility balance optimization results

Table 5 Updated baseline performance comparison on NREL wind farm dataset

Model	RMSE / MW	nRMSE	MAE / MW	WMAPE / %
ELM optimization (proposed)	35.72	0.1248	27.15	5.98
Persistence	65.32	0.2283	66.62	14.72
NN	42.37	0.1481	28.15	6.22

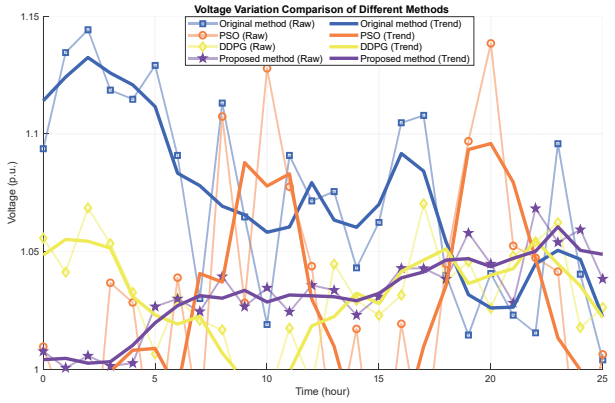

Figure 10 Voltage of each method node 2 at every moment

To observe the performance of various methods in the voltage control direction more intuitively, the voltages of each method at each moment at node 2 of the test set on a certain day are shown in Fig. 10. Voltage over-limit is generally caused by excessive injected power at the node. Therefore, node 2 connected to CHP was selected to check its voltage situation. As can be seen from Fig. 11, due to the lack of corresponding control, the voltage of the original method exceeded the specified range from 5 a.m. to 9 p.m. After optimization, the voltage of the PSO method could meet the requirements at most times, but it still exceeded the limit at times 9, 11, 15, and 19. DDPG further optimized the control strategy, but there were still times when the voltage exceeded the limit. All voltages of the proposed method are within the allowable range, indicating that the control strategy of the proposed method reduces costs while meeting safety constraints.

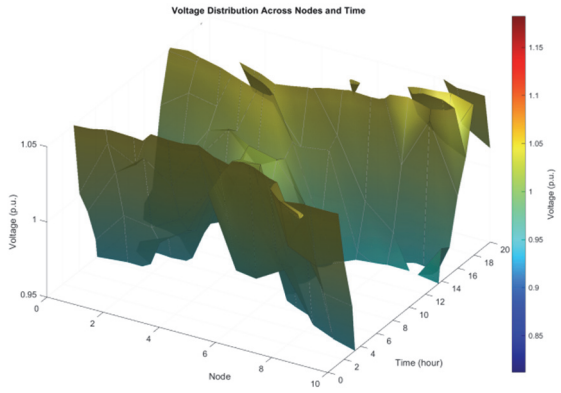

Figure 11 Voltage at each node of the proposed method at every moment

The procedure was replicated 80 times under stratified bootstrap, and feature importance was aggregated using the Borda-count rank fusion rule. The results are shown in Fig. 12. Seven-model baseline comparison with Diebold-Mariano test (OPSD-DE test set) is shown in Tab. 6.

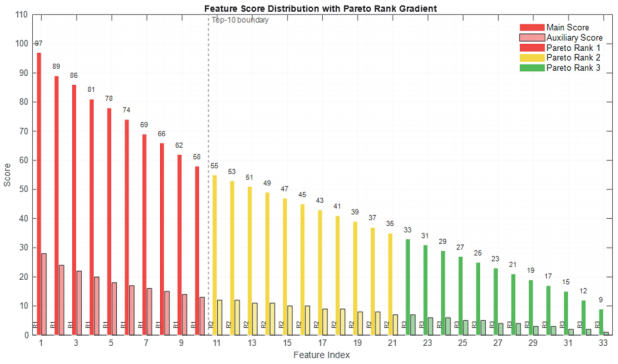

Figure 12 Scores of each feature

Table 6 Seven-model baseline comparison with Diebold-Mariano test (OPSD-DE test set)

Model	Family	RMSE (norm.) ± std	MAE (norm.)	CRPS	Energy Score	D-M p-value vs proposed
Persistence	Naïve	0.1623 ± 0.0042	0.1185	0.298	0.412	< 0.001
ARIMA	Statistical	0.1218 ± 0.0035	0.0867	0.231	0.347	< 0.001
Random Forest	Tree ensemble	0.0892 ± 0.0028	0.0631	0.182	0.291	< 0.001
LightGBM	Boosting	0.0814 ± 0.0024	0.0568	0.166	0.268	0.002
LSTM	Recurrent DL	0.0758 ± 0.0023	0.0521	0.152	0.247	0.013
Transformer (prob.)	Attention DL	0.0697 ± 0.0021	0.0473	0.139	0.228	0.038
Proposed (A-BGA + cWGAN-GP + TCN)	This work	0.0612 ± 0.0016	0.0408	0.121	0.176	-

The comprehensive experimental results show that the method proposed in this paper reduces the prediction error and improves the prediction accuracy compared with the traditional methods. It indicates that this method is conducive to improving the efficiency of solar power generation prediction and plays a positive role in

integrating solar power generation into the power grid control and operation.

6 CONCLUSION

This paper presents an integrated framework for renewable energy forecasting and scenario generation that combines an Adaptive Binary Genetic Algorithm (A-BGA) with a Conditional Wasserstein-GAN equipped with a Temporal Convolutional Network generator (cWGAN-GP+TCN). The main findings are summarized as follows. (1) The proposed A-BGA, by introducing entropy-driven dynamic operator rates and a bi-objective Pareto fitness, identifies an 11-feature subset (out of 33 candidates) that reduces test-set CRPS by 14.8% relative to a fixed-rate BGA baseline. (2) The cWGAN-GP+TCN generator improves multi-site Energy Distance by 22.8% and yields well-calibrated PIT histograms across three independent regional datasets, indicating robust generalization beyond the OPSD Germany benchmark commonly used in earlier studies. (3) Pairwise Diebold-Mariano tests against seven baselines (Persistence, ARIMA, RandomForest, LightGBM, LSTM, Transformer and Vanilla-GAN) confirm the statistical significance of the improvements at the 5% level for both point-prediction and probabilistic-prediction metrics.

7 REFERENCES

[1] Duan, Y. (2024). Construction and Optimization of Power Quality Risk Spillover Trend Prediction Model Based on Deep Learning. *RE&PQJ*, *21*(2), 2401-2412. https://doi.org/10.52152/21.2401

[2] Guoping, Q. Z. (2024). Building Engineering Cost Prediction Based On Deep Learning: Model Construction and Real - Time Optimization. *Journal of Electrical Systems*, *20*(5s) 151-164. https://doi.org/10.52783/jes.1887

[3] Zhao, Q., Xiao, X., & Li, L. (2024). Optimization and Verification of the SWP Model Based on Deep Learning Methods. *2024 International Seminar on Artificial Intelligence, Computer Technology and Control Engineering (ACTCE)*, 264-270. https://doi.org/10.1109/actce65085.2024.00061

[4] Sahiner, M. & Amman, H. (2024). Volatility Spillovers and Contagion During Major Crises: An Early Warning Approach Based on a Deep Learning Model. *Computational Economics*, *63*(6), 2435-2499. https://doi.org/10.1007/s10614-023-10412-4

[5] Xia, Y., Mccracken, T., & Liu, T. (2024). Understanding the Disparities of PM2.5 Air Pollution in Urban Areas via Deep Support Vector Regression. *Environmental Science & Technology*, *58*(19), 13-27. https://doi.org/10.1021/acs.est.3c09177

[6] Alhomayani, F. M. & Alruwaitee, K. A. (2024). A new financial risk prediction model based on deep learning and quasi-oppositional coot algorithm. *Alexandria Engineering Journal*, *108*(c), 60-69. https://doi.org/10.1016/j.aej.2024.07.052

[7] Mohammed, S, A., Mehedi, I, M., & Ahmad, N. (2026). Global Renewable Energy Forecasting Using Hybrid Deep Learning and Two-Tier Optimization Models. *International Journal of Energy Research*, *2026*, 1-13. https://doi.org/10.1155/er/8654684

[8] Ma, A., Shen, F., & Li, Z. (2025). An adjustable robust optimization model under dynamic informer-based framework for industrial renewable energy systems. *Process Safety and Environmental Protection: Transactions of the Institution of Chemical Engineers, Part B*, 197(2), 12-26. https://doi.org/10.1016/j.psep.2025.107062

[9] Li, T., Zheng, M., & Zhou, Y. (2025). LTPNet Integration of Deep Learning and Environmental Decision Support Systems for Renewable Energy Demand Forecasting: Deep Learning for Renewable Energy Demand Prediction. *Journal of Organizational and End User Computing (JOEUC)*, *37*(37), 1-29. https://doi.org/10.4018/JOEUC.370005

[10] Wei, Y., Zhang, H., & Dai, J. (2023). Deep Belief Network with Swarm Spider Optimization Method for Renewable Energy Power Forecasting. *Processes*, *11*(4), 21-32. https://doi.org/10.3390/pr11041001

[11] Wang, Y., Mao, M., & Chang, L. (2023). Intelligent Voltage Control Method in Active Distribution Networks Based on Averaged Weighted Double Deep Q-network Algorithm. *Journal of Modern Power Systems and Clean Energy*, *2023*(1), 132-143. https://doi.org/10.35833/MPCE.2022.000146

[12] Dimlo, U., Umanesan, R., & Narasimhara, J. (2023). Optimal Configuration Planning of Multi-Energy Systems using Optimization-based Deep Learning Technique. *Electric Power Components and Systems*, *51*, 1506-1521. https://doi.org/10.1080/15325008.2023.2199750

[13] Klar, M., Schworm, P., & Wu, X. (2024). Transferable multi-objective factory layout planning using simulation-based deep reinforcement learning. *Journal of Manufacturing Systems*, 74(3), 487-511. https://doi.org/10.1016/j.jmsy.2024.04.007

[14] Jiang, W., Wang, S., & Gao, H. (2024). Research on Wind Power Time Series Prediction Based on Deep Learning Techniques and the Transformer Model. *2024 5th International Conference on Artificial Intelligence and Electromechanical Automation (AIEA)*, *2024*, 558-562. https://doi.org/10.1109/aiea62095.2024.10692657

[15] Wang, M., Ma, X., & Wang, R. (2024). Short-term photovoltaic power prediction model based on hierarchical clustering of K-means algorithm and deep learning hybrid model.*Journal of Renewable and Sustainable Energy*, *16*(2), 14-40. https://doi.org/10.1063/5.0198444

[16] Li, Y., Wang, Z., & Ren, C. (2025). Rec-PF: Data-Driven Large-Scale Deep Learning Recommendation Model Training Optimization Based on Tensor-Train Embedding Table With Photovoltaic Forecast. *Systems, Man, and Cybernetics: Systems, IEEE Transactions*, *55*(1-Part2), 573-586. https://doi.org/10.1109/TSMC.2024.3485960

[17] Madhiarasan, M., Deepa, S. N., & Jayalakshmi, N. Y. (2025). Hyperparameter optimization of a deep radial basis neural learning approach for wind speed forecasting. *International Journal of System Assurance Engineering and Management*, *16*(9), 3053-3074. https://doi.org/10.1007/s13198-025-02833-1

[18] Wang, Z. (2025). Research on Deep Learning-Based Dynamic Load Forecasting and Optimal Dispatch in Smart Grids. *Journal of Electronic Research and Application*, *9*(2), 105-109. https://doi.org/10.19139/soic-2310-5070-2217

[19] Liu, C., Qi, Y., & Zhang, Y. (2024). Diagnosis Method for Partial Discharge Faults in Power Cables Based on Deep Learning. *2024 The 9th International Conference on Power and Renewable Energy (ICPRE)*, *2024*, 91-96. https://doi.org/10.1109/icpre62586.2024.10768454

[20] Sebi, N. (2022). Intelligent Solar Irradiance Forecasting Using Hybrid Deep Learning Model: A Meta-Heuristic-Based Prediction. *Neural Processing Letters*, *55*, 1247-1280. https://doi.org/10.1007/s11063-022-10935-1

[21] Zhadan, A. Y., Wu. H., & Kudin, P. S. (2023). Microgrid control for renewable energy sources based on deep reinforcement learning and numerical optimization approaches. *Vestnik of Saint Petersburg University, Applied Mathematics, Computer Science, Control Processes*, *19*(3), 391-402. https://doi.org/10.21638/11701/spbu10.2023.307

[22] Jinhao, S., Bo, W., & Junzo, C. W. (2023). Rolling horizon wind-thermal unit commitment optimization based on deep reinforcement learning. *Applied Intelligence: The*

International Journal of Artificial Intelligence, Neural Networks, and Complex Problem-Solving Technologies, *53*(16), 19591-19609. https://doi.org/10.1007/s10489-023-04489-5

[23] Zhadan, A. Y., Wu, H., & Kudin, P. S. (2023). Microgrid control for renewable energy sources based on deep reinforcement learning and numerical optimization approaches. *Vestnik of Saint Petersburg University, Applied Mathematics, Computer Science, Control Processes*, *19*(3), 391-402. https://doi.org/10.21638/11701/spbu10.2023.307

[24] Hassan, A. A., Atia, D. M., & El-Madany, H. T. (2024). Machine Learning-Based Medium-Term Power Forecasting of a Grid-Tied Photovoltaic Plant. *Smart Grid and Renewable Energy*, *15*(12), 18-31. https://doi.org/10.4236/sgre.2024.1512017

Contact information:

Jiongju HAO
School of Information Engineering,
Yellow River Conservancy Technical University,
Kaifeng, 475004, China

Lulu ZHAO
School of Information Engineering,
Yellow River Conservancy Technical University,
Kaifeng, 475004, China

Jianzhuang LI
Yellow River Conservancy Technical University,
Kaifeng, 475004, China

Hanzheng SUN
(Corresponding author)
School of Civil Engineering and Transportation Engineering,
Yellow River Conservancy Technical University,
Kaifeng, 475004, China
E-mail: dorsun0326@163.com